PLOS ONE

RESEARCH ARTICLE

Perturbed neurochemical and microstructural organization in a mouse model of prenatal opioid exposure: A multi-modal magnetic resonance study

Syed Salman Shahid[1]*, **Gregory G. Grecco**[2,3], **Brady K. Atwood**[2,4], **Yu-Chien Wu**[1,4]

1 Department of Radiology and Imaging Sciences, Indiana University School of Medicine, Indianapolis, IN, United States of America, **2** Department of Pharmacology and Toxicology, Indiana University School of Medicine, Indianapolis, IN, United States of America, **3** Medical Scientist Training Program, Indiana University School of Medicine, Indianapolis, IN, United States of America, **4** Stark Neurosciences Research Institute, Indiana University School of Medicine, Indianapolis, IN, United States of America

* shahids@iu.edu

Citation: Shahid SS, Grecco GG, Atwood BK, Wu Y-C (2023) Perturbed neurochemical and microstructural organization in a mouse model of prenatal opioid exposure: A multi-modal magnetic resonance study. PLoS ONE 18(7): e0282756. https://doi.org/10.1371/journal.pone.0282756

Editor: Tosin Abiola Olasehinde, University of Kwazulu-Natal, SOUTH AFRICA

Received: February 21, 2023

Accepted: July 8, 2023

Published: July 20, 2023

Data Availability Statement: The data generated and analyzed for the current study are within the paper and its Supporting Information file.

Funding: This work was supported in part by the Stark Neurosciences Research Institute, Indiana University (Brady K. Atwood) and NIH/NIAAA F30 AA028687 (Gregory G. Grecco). The funders had no role in the study design, data collection and analysis, decision to publish, or preparation of the manuscript.

Abstract

Methadone-based treatment for pregnant women with opioid use disorder is quite prevalent in the clinical environment. A number of clinical and animal model-based studies have reported cognitive deficits in infants prenatally exposed to methadone-based opioid treatments. However, the long-term impact of prenatal opioid exposure (POE) on pathophysiological mechanisms that govern neurodevelopmental impairment is not well understood. Using a translationally relevant mouse model of prenatal methadone exposure (PME), the aim of this study is to investigate the role of cerebral biochemistry and its possible association with regional microstructural organization in PME offspring. To understand these effects, 8-week-old male offspring with PME (n = 7) and prenatal saline exposure (PSE) (n = 7) were scanned in vivo on 9.4 Tesla small animal scanner. Single voxel proton magnetic resonance spectroscopy (^{1}H-MRS) was performed in the right dorsal striatum (RDS) region using a short echo time (TE) Stimulated Echo Acquisition Method (STEAM) sequence. Neurometabolite spectra from the RDS was first corrected for tissue T1 relaxation and then absolute quantification was performed using the unsuppressed water spectra. High-resolution in vivo diffusion MRI (dMRI) for region of interest (ROI) based microstructural quantification was also performed using a multi-shell dMRI sequence. Cerebral microstructure was characterized using diffusion tensor imaging (DTI) and Bingham-neurite orientation dispersion and density imaging (Bingham-NODDI). MRS results in the RDS showed significant decrease in N-acetyl aspartate (NAA), taurine (tau), glutathione (GSH), total creatine (tCr) and glutamate (Glu) concentration levels in PME, compared to PSE group. In the same RDS region, mean orientation dispersion index (ODI) and intracellular volume fraction (VF_{IC}) demonstrated positive associations with tCr in PME group. ODI also exhibited significant positive association with Glu levels in PME offspring. Significant reduction in major neurotransmitter metabolites and energy metabolism along with strong association between the neurometabolites and perturbed regional microstructural complexity suggest a possible

Competing interests: The authors have declared that no competing interests exist.

impaired neuroadaptation trajectory in PME offspring which could be persistent even into late adolescence and early adulthood.

Introduction

As the opioid epidemic has progressed over the past two decades, opioid use disorder has increased in pregnant women leading to an alarming rise in the number of babies being born with prenatal opioid exposure (POE) and undergoing neonatal opioid withdrawal [1–3]. Prenatal exposure to opioids produces adverse health consequences at birth with substantial neurobehavioral disruptions that persist at least into adolescence if not longer [2–4]. Clinical neuroimaging studies reveal macrostructural and morphometric disturbances in infants with POE, as well as profound alterations in functional connectivity [5]. However, there are substantial differences in the outcomes reported in clinical studies, likely due to the interaction of POE with environmental factors [4]. Animal models of POE are therefore especially valuable to disentangle environmental factors from the effects of the POE itself.

In order to elucidate the effects of POE on neurobehavioral outcomes, we developed a mouse model of POE that mimics a clinical scenario wherein a woman dependent on prescription painkillers (in this case oxycodone) undergoes medication-assisted therapy using methadone and then subsequently becomes pregnant [6]. Clinically, methadone is one of the highest sources of prenatal methadone exposure (PME) [7, 8]. Our PME model recapitulates many of the phenotypes associated with POE. Our previous studies have reported very high methadone levels in fetuses with a precipitous drop in neonates, the expression of neonatal opioid withdrawal, as well as a variety of neurological and behavioral disturbances as a result of PME [6, 9–11]. Using prenatal rodent models of opioid exposure, several studies have also reported neurodevelopmental alterations in the offspring of the exposed animals [12]. However, preclinical neuroimaging studies on opioid exposure are rather limited. To the best of our knowledge, there are only six rodent neuroimaging studies to date which have reported no macrostructural changes [6], alterations in major white matter tracts [13], widespread microstructural changes [9, 14] and changes in cerebral metabolites [15, 16].

We recently performed a neuroimaging assessment of our PME mice where we demonstrated the efficacy of diffusion magnetic resonance imaging (dMRI) in identifying widespread changes in microstructure due to PME [9]. Even though, our previous study demonstrated the sensitivity of model based dMRI to methadone mediated microstructural alterations in offspring, nevertheless, dMRI is limited in its ability to distinguish different tissue sub compartments. Additionally, water diffusion based quantitative MR methods cannot provide cell specific information on the affected tissue [17]. There is a knowledge gap regarding the cellular mechanisms that may be the driving factor for the microstructural development or the breakdown of regional structural integrity. Pathology specific alterations in cerebral metabolite levels have been associated with neurite microstructural alterations [18–20], therefore, it is imperative to investigate the association between POE-mediated cerebral metabolism and microstructural alterations.

In this multimodal in vivo MR study, we acquired dMRI, quantitative T1 and single voxel MRS data. Since neurodevelopmental processes are regulated by specific cell types and their corresponding microstructures, integrating these microstructural tissue properties with T1 relaxation compensated neurometabolites may provide important cell-specific information on the substrate of the cerebral tissue affected by the opioid exposure. We hypothesize that opioid

mediated neurodevelopmental changes will influence the regional neurochemistry. We further hypothesize that cerebral metabolite profile will exhibit varying degree of association with regional neurite microstructure in PME offspring. Such a multimodal approach can improve our understanding on the relationship between disturbed cerebral metabolite levels and associated neurite microstructural disorganization. In this study, we are specifically focusing on the dorsal striatum as we have previously identified disrupted neurophysiological processes and biochemical alterations in this brain region [6, 10, 11]. Given the role of dorsal striatum in regulating addiction related behavior and motor control in PME mice [21, 22], it is highly likely that disturbed physiological and neurometabolic changes in this region contribute to the observed behavioral disturbances.

Material and methods

Animal preparation

Our previous protocol was used to produce mice with PME [6]. Briefly, single-housed adult female C57Bl/6J (Jackson Labs, Bar Harbor, ME) mice were treated with either saline (10 ml/kg, s.c. b.i.d.) or an escalating dose treatment with oxycodone (10 mg/kg to 30 mg/kg, s.c.b.i.d.) over the course of 8 days. These oxycodone-treated females were then transferred to methadone treatment (10 mg/kg, s.c.b.i.d.). 5 days after switching to methadone the females were mated with an 8-week-old C57Bl/6J male mouse. These mice continued to receive the same dose of methadone throughout pregnancy and until PME offspring were weaned at postnatal day 28. Saline-treated mice continued to be treated with saline throughout pregnancy to produce prenatal saline exposure (PSE) offspring. Offspring were housed 2–4 mice/cage until neuroimaging was performed at 8–9 weeks of age as previously indicated [9].

All experiments performed with dams, sires, and offspring followed the National Institutes of Health guidelines for the usage of laboratory animals and experimental protocols were approved by the Indiana University School of Medicine Institutional Animal Care and Use Committee. All ARRIVE guidelines were also followed [23].

MR acquisition

For MR experiments, 7 animals from each group were imaged. Initially animals were anesthetized under 3% isoflurane in an induction chamber. The anesthetized mice were transferred to an MR compatible cradle and positioned in an MRI compatible head holder to minimize head motion. Anesthesia was then maintained at 1.5% isoflurane in 100% oxygen throughout imaging. Respiration rate was monitored using a pressure pad placed under the animal abdomen and animal body temperature was maintained by a warming pad (37˚C) placed under the animal. The in vivo imaging was conducted on a horizontal bore 9.4 Biospec pre-clinical MRI system (Bruker BioSpin MRI GmbH, Germany) equipped with shielded gradients (maximum gradient strength = 660 mT/m, rise time = 4750 T/m/s). An 86 mm quadrature volume resonator was used for transmission and a 4-element array cryocoil was used for signal reception (cryoprobe, Bruker, BioSipn). For dMRI, a 2D multi-shell diffusion acquisition scheme was used. The DWIs were acquired using a segmented dual spin-echo echo planar imaging (EPI) sequence using the following parameters: TE/TR = 35.84/3000 ms, δ/Δ = 3/15 ms, matrix size = 128 × 125, voxel size = 130 × 130x130 μm^3, number of slices = 40, slice thickness = 130 μm, 2 b-value shells (1000 and 2000) s/mm^2, 10 b0 (5 for each shell), 32 diffusion encoding direction for b = 1000 and 56 for b = 2000 s/mm^2. A high-resolution FLASH based multi-slice 2D anatomical reference image was acquired to facilitate MRS voxel (1.8 mm^3) placement in the right dorsal striatum (Fig 1A and 1B). The reference scan was acquired using the following acquisition parameters: TE/TR = 3/15ms, slice thickness = 500 μm, in-

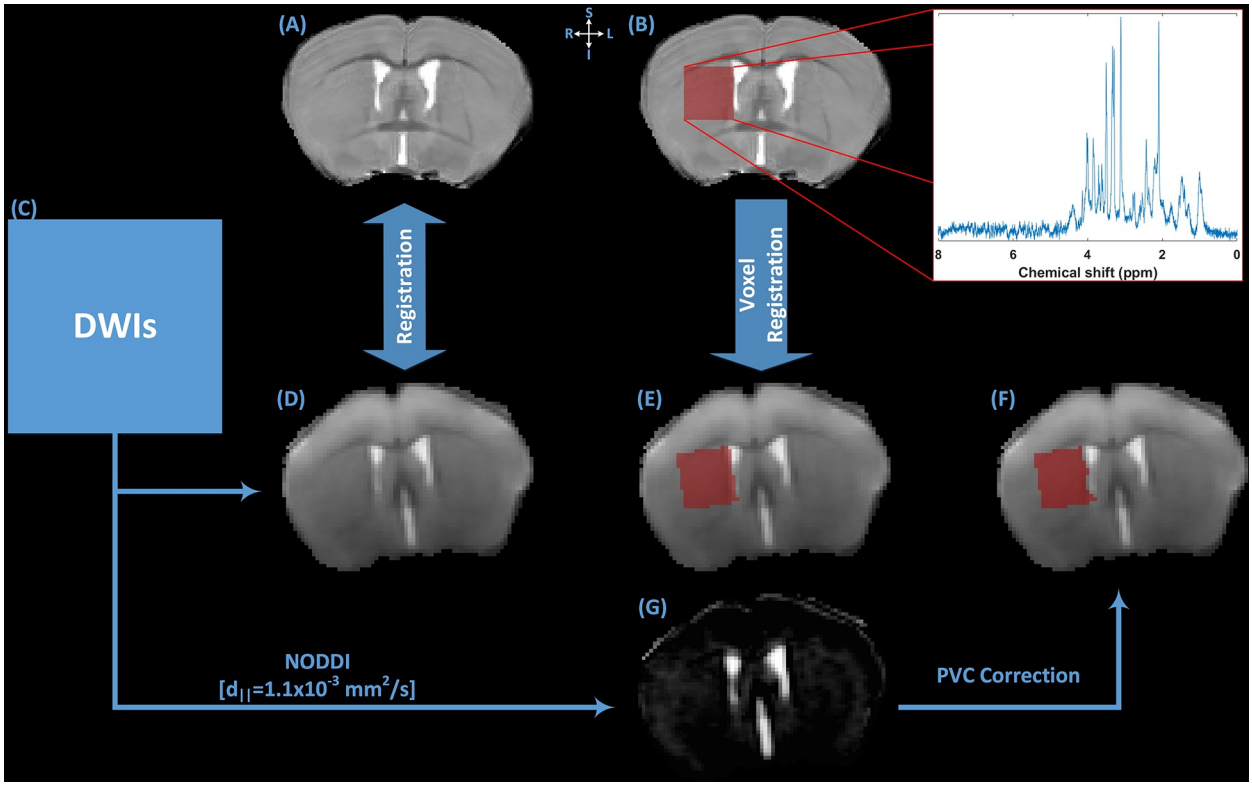

Fig 1. The schematics of the MR image processing framework used in the study. (A) T2-weighted anatomical reference image was used for the manual placement of a 1.8 mm^3 voxel in the right dorsal striatum region of the animal. (B) T2-weighted anatomical reference image with voxel mask in the right DSR, Inset shows the raw water-suppressed ^{1}H-MR spectrum from the single voxel location. (C) DWIs were used to extract averaged b0 image and NOODI derived parametric maps of microstructure. (D) b0 image was linearly register to (A) T2-weighted anatomical reference image. Localized voxel location from (B) T2-weighted anatomical reference image was mapped to subject's diffusion space using (E) averaged b0 image. (G) Cerebrospinal fluid (CSF) partial volume contamination (PVC) was estimated from NODDI derived VF_{CSF} parameter. (F) CSF PVC was corrected in the mapped voxel. Using the corrected voxel mask, mean values of microstructural parametric maps were calculated for further analysis.

https://doi.org/10.1371/journal.pone.0282756.g001

plane voxel resolution = 78x78 μm^2, number of slices = 20, number of averages = 3, matrix size = 192x192, flip angle = 10˚. To understand the potential contribution of tissue T1 relaxation time on metabolic quantification, a single slice T1 map was acquired. The location of the FoV overlapped with the MRS voxel location. T1 map acquisition is based on single slice Fluid attenuation inversion recovery technique with EPI (FLAIR_EPI), with the following acquisition parameters: TE = 17ms, Recovery time = 10000ms, slice thickness = 1000 μm, repetition time (TI) = [30, 100, 200, 300, 400, 500, 600, 700, 800, 900, 1000, 1100, 1400, 1700, 2000, 2300, 2600, 2900, 3200, 3500] ms, matrix size = 128x96 and inversion slab thickness = 4.0 mm.

The single voxel spectra (SVS) were acquired with a Stimulated Echo Acquisition Method (STEAM) spectroscopy sequence. A 1.8 mm^3 voxel was manually placed in the right dorsal striatum using the acquired anatomical reference Scan (Fig 1B). Before the spectra acquisition, automated localized shimming was performed using Bruker provided FASTMAP method. The field was shimmed to $<$ 15 Hz Full Width Half Maximum (FWHM) linewidth of the unsuppressed water peak. The following parameters were used for spectra acquisition: TE = 4ms, mixing time (TM) = 10ms, TR = 2500 ms, 2048 complex data points, spectral width = 4000Hz, Outer volume suppression (OVS) enabled, and water signal suppression was achieved using variable power and optimized relaxation delays (VAPOR) scheme. OVS slice thickness = 5mm, gap to voxel = 1 mm, number of dummy scans = 8, number of averages = 384.

An additional SVS was acquired as a reference for absolute metabolic quantification using the same acquisition parameters as above except without water suppression enabled. The number of averages for unsuppressed spectra was 10.

MR data processing

The pre- and post-processing methodologies pertaining to dMRI is described elsewhere [9]. Briefly, the raw DWIs were denoised [24], brain segmented [25], motion and eddy current induced geometric distortion corrected [26] and B1 field inhomogeneity corrected [27]. For dMRI model fitting, voxel-based diffusion tensor imaging was performed uing '*DTIFIT*' function in FMRIB Software Library (FSL v6.0) [28] using DWI data from b = 0 and 1000 s/mm^2. Multi-compartment microstructural imaging was performed using Bingham-NODDI model [29]. The high-resolution anatomical reference image was denoised using Non-local Means (*NLMeans*) filter implemented in ANIMA (https://anima.irisa.fr) [30]. Using a custom-built python script, the MRS voxel location was mapped on the reference image (Fig 1B). To extract microstructural parameters from the MRS voxel location, the denoised reference image was skull stripped [25], bias field corrected [31] and then linearly registered to the b0 image in the diffusion space (Fig 1A, 1C and 1D). Using the resulting transformation matrix, MRS voxel mask was translated to b0 image space (Fig 1B and 1E). Within the MRS voxel, Cerebrospinal fluid (CSF) partial volume contamination (PVC) was estimated from NODDI derived VF_{CSF} map (Fig 1G) and image voxels, within MRS voxel, containing PVC were removed (Fig 1F). This PVC corrected MRS voxel mask was used to extract total MRS voxel volume and mean values of ODI, V_{ISO}, VF_{IC} and VF_{EC} using the FSL '*fslstats*' tool (S1 Table in S1 File). T1 relaxation parameters were estimated on Paravision 360 '*Image sequence analysis*' tool using a square region of interest (1.8x1.8 mm^2) at the approximate location of the MRS voxel with the default settings.

LC Model [32] was used for spectral fitting and absolute metabolite quantification (Fig 2). Before quantification, the raw water suppressed spectra was inspected for poor water suppression, lipid contamination and motion artefacts. The basis-set included model spectra for alanine (Ala), aspartate (Asp), creatine (Cr), phosphocreatine (PCr), γ-aminobutyric acid (GABA), glucose (Glc), glutamine (Gln), glutamate (Glu), glutathione (GSH), glycerophosphpcholine (GPC), phosphocholine (PCh), myo-inositol (mIns), lactate (Lac), N-acetyl aspartate (NAA), N-acetylaspartylglutamate (NAAG), scyllo-inositol (Scyllo) and taurine (Tau). Absolute quantification was performed using the unsuppressed water spectra as a reference. Correction factor related CSF PVC and T1 relaxation of water were also introduced in absolute metabolite quantification. The reliability of the measured metabolite concentration was estimated by Cramer-Rao lower bounds (CRLB) and only those metabolites with CRLB $< 15\%$ were selected for further analysis. The metabolite concentrations are reported in μmol/g. PCh and GPC were expressed as total choline (tCh) and Cr and PCr were expressed as total creatine (tCr).

Statistical analysis

To investigate group differences in absolute metabolite concentrations, independent T-test with general linear model (GLM) was used. Benjamini-Hochberg false discovery rate (FDR) correction was used to account for multiple comparison and $p_{FDR} < 0.05$ was deemed significant. To evaluate the relationship between neurochemical levels and microstructural indices in the same region-of-interest (i.e., RDS), partial correlation analyses were performed, and PVC MRS voxel volume was included as a covariate. The analyses were performed in SPSS (IBM SPSS, Version 27).

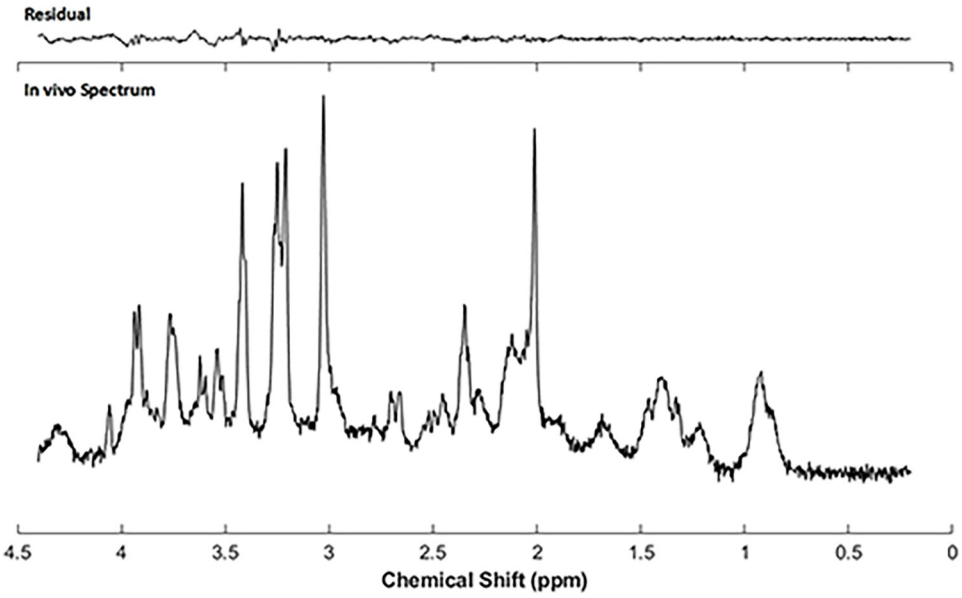

Fig 2. A representative single voxel ^{1}H-MR spectrum from a PME mouse using a short echo (TE = 4ms) STEAM sequence at 9.4 T. the In vivo ^{1}H single voxel magnetic resonance spectrum was obtained using a 1.8 mm^{3} isotropic voxel located in right dorsal striatum region of the animal. Spectrum quantification was performed using LC Model. Quantification reliability was estimated using Cramer-Rao lower bounds (CRLB). Metabolite data with CRLB > 15% were considered unreliable and exclude from analysis.

https://doi.org/10.1371/journal.pone.0282756.g002

In order to assess the role of neurometabolites on microstructural organization, we conducted partial correlation analyses between regional metabolite concentration levels and the microstructural parameters in PSE and PME groups, separately. For each correlation analysis, PVC corrected MRS voxel volume was considered as a covariate. Furthermore, to test, whether the respective correlations in intra-group associations are significantly different from each other, we transformed the individual correlations to Fisher Z scores. Z scores were compared and analyzed for statistical significance by calculating the observed z test statistics ($Z_{Observed}$) [33].

Results

Effect of prenatal methadone exposure on cerebral metabolites

Significant group differences between PSE and PME offspring were observed across a number of neurometabolite concentration levels in the RDS (Table 1). PME offspring exhibited significantly lower concentration levels of NAA ($p_{FDR} < 0.05$; Cohens'd = 1.83; 95% CI: 0.53–3.08), Tau ($p_{FDR} < 0.05$; Cohens'd = 1.63; 95% CI: 0.37–2.83), GSH ($p_{FDR} < 0.05$; Cohens'd = 1.60; 95% CI: 0.35–2.81), tCr ($p_{FDR} < 0.05$; Cohens'd = 1.52; 95% CI: 0.29–2.70) and Glu ($p_{FDR} < 0.05$; Cohens'd = 1.43; 95% CI: 0.21–2.59).

Cerebral metabolite associations with neurite microstructure

Table 2 show the partial correlation between the regional metabolite concentration levels and diffusion microstructural indices in PME group. Total creatine exhibited strong positive associations with regional ODI ($r = 0.89$, $p < 0.05$) and with regional VF_{IC} ($r = 0.87$, $p < 0.05$). Glu was negatively associated with regional mean diffusivity ($r = -0.92$, $p < 0.01$) and was positively associated with regional ODI ($r = 0.94$, $p < 0.01$). After FDR correction for multiple

Table 1. Comparison of neurometabolite concentrations in right dorsal striatum measured by ^{1}H-MRS (n = 7 per group).

Metabolites [μmol/g]	Mean difference PSE-PME	p_{FDR}	Effect size (Cohen's d)	95% Confidence Interval
NAA	0.87	**0.03**	1.83	0.53–3.08
Tau	1.73	**0.03**	1.63	0.37–2.83
GSH	0.28	**0.03**	1.60	0.35–2.81
tCr	0.89	**0.03**	1.52	0.29–2.70
Glu	0.94	**0.04**	1.43	0.21–2.59
Gln	0.36	0.08	1.14	-0.02–2.26
GABA	0.11	0.30	0.67	-0.42–1.74
Ins	0.29	0.31	0.61	-0.47–1.67
tCh	0.02	0.68	0.23	-0.83–1.27

Abbreviations: n = number of animals, PSE = postnatal saline exposure, PME = postnatal methadone exposure, NAA = N-acetylaspartate, Tau = taurine, GSH = glutathione, tCr = total creatine (Cr+PCr), Glu = glutamate, Gln = glutamine, GABA = γ-aminobutyric acid, Ins = myo-inositol, tCh = total choline (GPC + PCh). *p* values in bold survived false-discovery rate (FDR) correction for multiple comparison at $p_{FDR}<0.05$ using Benjamini-Hochberg criterion (α = 0.05).

https://doi.org/10.1371/journal.pone.0282756.t001

comparison, Glu–ODI association remained statistically significant ($p_{FDR} < 0.05$). No significant correlations were observed between regional neurometabolite levels and regional microstructural parameters in the combined groups (PME+PSE; See S2 Table in S1 File) or in the PSE group alone (S3 Table in S1 File).

Discussion

The study employed short echo time STEAM ^{1}H-MRS sequence to obtain regional neurochemical profile and used multi-shell dMRI, aided with multi-compartment diffusion modeling, to extract quantitative information related to regional microstructural organization. Using highly resolved short TE spectra, we successfully quantified various intracellular metabolite concentrations, thus were able to probe PME associated biochemical alterations. With these advanced imaging tools, the present study investigated the differences in cerebral metabolite concentration levels in the right dorsal striatum region between PSE and PME offspring at 8 weeks of age. In the PME offspring group, a significant decrease was observed in a number of

Table 2. Partial correlation between the neurometabolite concentrations and the diffusion microstructural metrices in the right dorsal striatum (PME).

Metabolites [μmol/g]	FA		MD (mm^2/s)		ODI		VF_{IC}	
	r	p value	r	p value	r	p value	r	p value
NAA	0.549	0.260	0.224	0.670	0.122	0.818	0.449	0.372
Tau	-0.530	0.279	-0.663	0.152	0.416	0.412	0.089	0.868
GSH	-0.092	0.862	-0.293	0.573	0.410	0.420	0.676	0.141
tCr	0.046	0.931	-0.786	0.064	0.891	**0.017**‡	0.873	**0.023**‡
Glu	-0.375	0.464	-0.924	**0.008**‡	0.939	**0.005***‡	0.741	0.092
Gln	0.741	0.092	0.351	0.495	-0.090	0.865	0.403	0.428
GABA	0.427	0.398	0.043	0.935	-0.084	0.875	0.273	0.601
Ins	0.062	0.908	-0.698	0.123	0.749	0.087	0.652	0.160
tCh	0.317	0.540	-0.649	0.163	0.715	0.110	0.686	0.132

Analysis adjusted for PVC corrected MRS voxel volume. *Denotes $p_{FDR} < 0.05$; ‡ denotes the respective correlations are significantly different between groups ($p<0.01$). Abbreviations: r = correlation coefficient, NAA = N-acetylaspartate, Tau = taurine, GSH = glutathione, tCr = total creatine (Cr+PCr), Glu = glutamate, Gln = glutamine, GABA = γ-aminobutyric acid, Ins = myo-inositol, tCh = total choline (GPC + PCh), FA = fractional anisotropy, MD = mean diffusivity, ODI = orientation dispersion index, VF_{IC} = intra-cellular volume fraction, PVC = Partial volume contamination.

https://doi.org/10.1371/journal.pone.0282756.t002

neurometabolites (including NAA, Taurine, Glutamate, glutathione and creatine) in the right dorsal striatum region compared to the PSE group. We further examined the relationship between regional neurochemistry and microstructural organization in PME offspring and found significant associations between neurometabolite levels and microstructural changes in the PME group. However, we did not find significant associations between neurometabolite concentration levels and microstructural parameters in the control group.

NAA, which is synthesized in mitochondria, is predominantly present in the neuronal component [34]. Higher NAA levels are associated with neuronal health and synaptic integrity [35–38]. Thus, NAA is considered a marker of neuronal integrity and function. The results of our study showed significantly lower levels of NAA in the dorsal striatum of PME group compared to control PSE group. A number of studies in aging [39], Alzheimer's disease pathology [40] and multiple sclerosis [41] have reported association between neuronal integrity and NAA levels. However, there is a strong argument that at brain maturation and development stage, changes in NAA levels maybe associated with the development of dendrites and synaptic connections [42, 43]. A recent pre-clinical MRS based study suggested that NAA might be a biomarker of neuronal insult after prenatal opioid exposure and subsequent withdrawal [16]. Based on the current evidence, it is possible that lower levels of NAA in PME offspring might be associated with withdrawal. Glutamate is a primary excitatory neurotransmitter in mammalian brain [44]. It is involved in memory and learning, synaptic plasticity, synaptic connections, neuronal growth and differentiation [45]. A number of studies have reported the influence of the dysfunctional glutamatergic system in mood disorders [46] and opioid dependence [47, 48]. Our results showed significant reduction in Glu levels in PME offspring, compared to PSE group. Although the reduction of Glu measured with MRS in PME offspring is from multiple neuronal and glial pools including many metabolic functions in addition to Glu's role in excitatory neurotransmission, this reduction in Glu could reflect an effect of opioid exposure on Glu synaptogenesis and Glu-mediated neurotransmission. Indeed a recent study by Grecco, Munoz [10] reported the impaired synaptic Glu signaling pathways in excitatory neurotransmission in the dorsal striatum of adolescent PME offspring. In agreement with healthy aging study [49], our results (S1 Fig in S1 File) also demonstrated strong positive correlation between Glu and NAA in PSE group, which supports the hypothesis that Glu is an indicator of synaptic health.

Taurine plays an important role in neurodevelopment [39]. The role of Tau in neurite proliferation, synaptogenesis and synaptic transmission is well documented [50]. In our study, Tau concentration levels were significantly lower in PME offspring compared to control group, suggesting long lasting effect of PME on Tau-mediated neuroadaptations related to neurodevelopment [15]. GSH is an antioxidant which is present in brain, primarily in astrocytes [51]. GSH is primarily implicated in oxidation-reduction reactions, serves as a protector against toxic agents such as reactive oxygen species (ROS) [52]. Alterations in cerebral GSH levels from opioid withdrawal mediated oxidative imbalance may reflect inflammatory processes and mitochondrial dysfunction [53, 54]. Our results demonstrated significant reduction in GSH concentration levels in RDS of PME offspring group, compared to the control group. This may suggest the long-lasting effect of methadone on cerebral oxidative imbalance in prenatally exposed offspring.

Total creatine plays a very significant role in cellular energy metabolism. In central nervous system, Cr and PCr are present in neurons and glial cells [55]. Alterations in cerebral tCr levels indicate mitochondrial dysfunction [56] and disturbed cerebral energy metabolism [57]. To date, there are conflicting reports on altered bioenergetics in human opioid and methadone maintenance therapy studies [47]. Our results indicate significant reduction of tCr levels in PME offspring, compared to control group. These results may suggest long lasting effects of

prenatal opioid exposure on cerebral bioenergetics. Furthermore, our results indicate that tCr should not be considered as an internal reference in PME studies due to significant group-wise alterations in its concentration levels. Moreover, the metabolite ratio is less sensitive when the concentration of both metabolites is affected by considered pathology.

Previous studies in healthy aging suggest the association between regional neurochemical composition and microstructural organization [58, 59]. In this study we observed a strong positive association between regional Glu levels and ODI in PME group. Interestingly, the trajectory of this association in PSE group was in opposite direction and was not statistically significant. Total Cr in PME group also exhibited positive associations with regional ODI and VF_{IC} parameters, although these correlations did not survive the FDR based corrections but do suggest the possible involvement of altered neurochemical composition in regulating neurite microstructural organization in PME offspring.

There are some limitations which need to be highlighted. Given the exploratory nature of the work, we only scanned male offspring. We also only scanned the right dorsal striatum, and other brain regions certainly warrant further investigation. In addition, the sample size was relatively small and therefore, generalization of these results should be considered with caution. Additionally due to the cross-sectional nature of the study design, it was not possible to establish cause and effect relationship between cerebral metabolites and microstructural parameters. In future, it would be interesting to repeat this work with a much larger sample size and at an early postnatal stage. Larger sample size will certainly be beneficial for such a multi-modal study and imaging at early postnatal period may show more pronounced effects due acute withdrawal. Other possibilities would be to include females in the study to examine the sex effects. We believe that the effects of prenatal opioid exposure are likely much more subtle compared to other agents such as alcohol which produces a more neurotoxic effect. As such, more advanced imaging modalities such as DWI and MRS (and multimodal studies) may be needed to parse out these subtle effects of prenatal opioid exposure on neurodevelopment. Despite these limitations, the study suggests that PME can significantly affect neurodevelopment in PME offspring by perturbing neurometabolism and brain microstructure and the effects of these perturbation can persist into late adolescent and early adulthood. Maybe this work will further support the utility of advanced neuroimaging techniques in studying the growing population of children with prenatal opioid exposure and perhaps these findings represent novel biomarkers which can assist in identifying children, with prenatal opioid-induced disruption of neurodevelopment, in need of further clinical intervention.

Supporting information

S1 File.
(DOCX)

S1 Data.
(CSV)

Acknowledgments

The authors would like to express their gratitude to Erin Jarvis for her assistance in animal preparation, scanning and care in MR data collection.

Author Contributions

Conceptualization: Syed Salman Shahid, Gregory G. Grecco, Brady K. Atwood, Yu-Chien Wu.

Data curation: Syed Salman Shahid.

Formal analysis: Syed Salman Shahid, Gregory G. Grecco, Yu-Chien Wu.

Funding acquisition: Gregory G. Grecco, Brady K. Atwood, Yu-Chien Wu.

Investigation: Syed Salman Shahid, Gregory G. Grecco, Brady K. Atwood, Yu-Chien Wu.

Methodology: Syed Salman Shahid, Gregory G. Grecco, Brady K. Atwood, Yu-Chien Wu.

Project administration: Gregory G. Grecco, Brady K. Atwood, Yu-Chien Wu.

Resources: Gregory G. Grecco, Brady K. Atwood, Yu-Chien Wu.

Software: Syed Salman Shahid.

Supervision: Syed Salman Shahid.

Validation: Syed Salman Shahid, Gregory G. Grecco.

Visualization: Syed Salman Shahid.

Writing – original draft: Syed Salman Shahid.

Writing – review & editing: Syed Salman Shahid, Gregory G. Grecco, Brady K. Atwood, Yu-Chien Wu.

References

1. Hirai A.H., et al., Neonatal Abstinence Syndrome and Maternal Opioid-Related Diagnoses in the US, 2010–2017. JAMA, 2021. 325(2): p. 146–155. https://doi.org/10.1001/jama.2020.24991 PMID: 33433576
2. Shatil B. and Landau R., Opioid Use and Misuse in Pregnancy. Clin Perinatol, 2020. 47(4): p. 769–777. https://doi.org/10.1016/j.clp.2020.08.004 PMID: 33153661
3. Cook J.L., Epidemiology of opioid use in pregnancy. Best Pract Res Clin Obstet Gynaecol, 2022. 85(Pt B): p. 12–17. https://doi.org/10.1016/j.bpobgyn.2022.07.008 PMID: 36045026
4. Conradt E., et al., Prenatal Opioid Exposure: Neurodevelopmental Consequences and Future Research Priorities. Pediatrics, 2019. 144(3). https://doi.org/10.1542/peds.2019-0128 PMID: 31462446
5. Radhakrishnan R., et al., Neuroimaging in infants with prenatal opioid exposure: Current evidence, recent developments and targets for future research. J Neuroradiol, 2021. 48(2): p. 112–120. https://doi.org/10.1016/j.neurad.2020.09.009 PMID: 33065196
6. Grecco G.G., et al., Prenatal methadone exposure disrupts behavioral development and alters motor neuron intrinsic properties and local circuitry. Elife, 2021. 10: p. e66230. https://doi.org/10.7554/eLife.66230 PMID: 33724184
7. MacMillan K.D.L., Neonatal Abstinence Syndrome: Review of Epidemiology, Care Models, and Current Understanding of Outcomes. Clin Perinatol, 2019. 46(4): p. 817–832. https://doi.org/10.1016/j.clp.2019.08.012 PMID: 31653310
8. Duffy C.R., et al., Trends and Outcomes Associated With Using Long-Acting Opioids During Delivery Hospitalizations. Obstet Gynecol, 2018. 132(4): p. 937–947. https://doi.org/10.1097/AOG.0000000000002861 PMID: 30204694
9. Grecco G.G., et al., Alterations of brain microstructures in a mouse model of prenatal opioid exposure detected by diffusion MRI. Sci Rep, 2022. 12(1): p. 17085. https://doi.org/10.1038/s41598-022-21416-9 PMID: 36224335
10. Grecco G.G., et al., Prenatal Opioid Exposure Impairs Endocannabinoid and Glutamate Transmission in the Dorsal Striatum. eNeuro, 2022. 9(2). https://doi.org/10.1523/ENEURO.0119-22.2022 PMID: 35396255
11. Grecco G.G., et al., Prenatal opioid exposure reprograms the behavioural response to future alcohol reward. Addict Biol, 2022. 27(2): p. e13136. https://doi.org/10.1111/adb.13136 PMID: 35229956

12. Byrnes E.M. and Vassoler F.M., Modeling prenatal opioid exposure in animals: Current findings and future directions. Front Neuroendocrinol, 2018. 51: p. 1–13. https://doi.org/10.1016/j.yfrne.2017.09.001 PMID: 28965857
13. Jantzie L.L., et al., Prenatal opioid exposure: The next neonatal neuroinflammatory disease. Brain Behav Immun, 2020. 84: p. 45–58. https://doi.org/10.1016/j.bbi.2019.11.007 PMID: 31765790
14. Hornburg K.J., et al., Prenatal heroin exposure alters brain morphology and connectivity in adolescent mice. NMR Biomed, 2023. 36(2): p. e4842. https://doi.org/10.1002/nbm.4842 PMID: 36259728
15. Odegaard K.E., et al., A Holistic Systems Approach to Characterize the Impact of Pre- and Post-natal Oxycodone Exposure on Neurodevelopment and Behavior. Front Cell Dev Biol, 2020. 8: p. 619199. https://doi.org/10.3389/fcell.2020.619199 PMID: 33490084
16. Ward P., et al., N-acetylcysteine mitigates acute opioid withdrawal behaviors and CNS oxidative stress in neonatal rats. Pediatr Res, 2020. 88(1): p. 77–84. https://doi.org/10.1038/s41390-019-0728-6 PMID: 31935745
17. Jones D.K., et al., Microstructural imaging of the human brain with a 'super-scanner': 10 key advantages of ultra-strong gradients for diffusion MRI. NeuroImage, 2018. 182: p. 8–38. https://doi.org/10.1016/j.neuroimage.2018.05.047 PMID: 29793061
18. Gozdas E., et al., 1H-MRS neurometabolites and associations with neurite microstructures and cognitive functions in amnestic mild cognitive impairment. NeuroImage: Clinical, 2022: p. 103159. https://doi.org/10.1016/j.nicl.2022.103159 PMID: 36063758
19. Caprihan A., et al., The paradoxical relationship between white matter, psychopathology and cognition in schizophrenia: a diffusion tensor and proton spectroscopic imaging study. Neuropsychopharmacology, 2015. 40(9): p. 2248–2257. https://doi.org/10.1038/npp.2015.72 PMID: 25786581
20. Kara F., et al., (1)H MR spectroscopy biomarkers of neuronal and synaptic function are associated with tau deposition in cognitively unimpaired older adults. Neurobiol Aging, 2022. 112: p. 16–26.
21. Everitt B.J. and Robbins T.W., From the ventral to the dorsal striatum: devolving views of their roles in drug addiction. Neuroscience & Biobehavioral Reviews, 2013. 37(9): p. 1946–1954.
22. Balleine B.W., Delgado M.R., and Hikosaka O., The role of the dorsal striatum in reward and decision-making. J Neurosci, 2007. 27(31): p. 8161–5. https://doi.org/10.1523/JNEUROSCI.1554-07.2007 PMID: 17670959
23. Kilkenny C., et al., Improving bioscience research reporting: the ARRIVE guidelines for reporting animal research. Journal of Pharmacology and Pharmacotherapeutics, 2010. 1(2): p. 94–99. https://doi.org/10.4103/0976-500X.72351 PMID: 21350617
24. Wiest-Daesslé N., et al. Rician noise removal by non-local means filtering for low signal-to-noise ratio MRI: applications to DT-MRI. in International Conference on Medical Image Computing and Computer-assisted Intervention. 2008. Springer.
25. Oguz I., et al., RATS: Rapid Automatic Tissue Segmentation in rodent brain MRI. J Neurosci Methods, 2014. 221: p. 175–82. https://doi.org/10.1016/j.jneumeth.2013.09.021 PMID: 24140478
26. Andersson J.L. and Sotiropoulos S.N., Non-parametric representation and prediction of single- and multi-shell diffusion-weighted MRI data using Gaussian processes. Neuroimage, 2015. 122: p. 166–76. https://doi.org/10.1016/j.neuroimage.2015.07.067 PMID: 26236030
27. Zhang Y., Brady M., and Smith S., Segmentation of brain MR images through a hidden Markov random field model and the expectation-maximization algorithm. IEEE Trans Med Imaging, 2001. 20(1): p. 45–57. https://doi.org/10.1109/42.906424 PMID: 11293691
28. Jbabdi S., et al., Model-based analysis of multishell diffusion MR data for tractography: how to get over fitting problems. Magn Reson Med, 2012. 68(6): p. 1846–55. https://doi.org/10.1002/mrm.24204 PMID: 22334356
29. Tariq M., et al., Bingham–NODDI: Mapping anisotropic orientation dispersion of neurites using diffusion MRI. NeuroImage, 2016. 133: p. 207–223. https://doi.org/10.1016/j.neuroimage.2016.01.046 PMID: 26826512
30. Coupe P., et al., An optimized blockwise nonlocal means denoising filter for 3-D magnetic resonance images. IEEE Trans Med Imaging, 2008. 27(4): p. 425–41. https://doi.org/10.1109/TMI.2007.906087 PMID: 18390341
31. Tustison N.J., et al., N4ITK: improved N3 bias correction. IEEE Trans Med Imaging, 2010. 29(6): p. 1310–20. https://doi.org/10.1109/TMI.2010.2046908 PMID: 20378467
32. Provencher S.W., Automatic quantitation of localized in vivo 1H spectra with LCModel. NMR Biomed, 2001. 14(4): p. 260–4. https://doi.org/10.1002/nbm.698 PMID: 11410943
33. Snedecor G.W. and Cochran W.G., Statistical Methods Iowa State University Press, Ames. Statistical methods, 7th ed. The Iowa State University Press, Ames, 1980: p. 117–192.

34. Gujar S.K., et al., Magnetic resonance spectroscopy. J Neuroophthalmol, 2005. 25(3): p. 217–26. https://doi.org/10.1097/01.wno.0000177307.21081.81 PMID: 16148633

35. Gill S., et al., Brain metabolites as 1H NMR markers of neuronal and glial disorders. NMR in biomedicine, 1989. 2(5-6): p. 196–200. https://doi.org/10.1002/nbm.1940020505 PMID: 2561957

36. Murray M.E., et al., Early Alzheimer's disease neuropathology detected by proton MR spectroscopy. J Neurosci, 2014. 34(49): p. 16247–55. https://doi.org/10.1523/JNEUROSCI.2027-14.2014 PMID: 25471565

37. Simmons M.L., Frondoza C.G., and Coyle J.T., Immunocytochemical localization of N-acetyl-aspartate with monoclonal antibodies. Neuroscience, 1991. 45(1): p. 37–45. https://doi.org/10.1016/0306-4522(91)90101-s PMID: 1754068

38. Petroff O.A., Pleban L., and Prichard J.W., Metabolic assessment of a neuron-enriched fraction of rat cerebrum using high-resolution 1H and 13C NMR spectroscopy. Magn Reson Med, 1993. 30(5): p. 559–67. https://doi.org/10.1002/mrm.1910300506 PMID: 7903113

39. Cichocka M. and Beres A., From fetus to older age: A review of brain metabolic changes across the lifespan. Ageing Res Rev, 2018. 46: p. 60–73.

40. Gao F. and Barker P.B., Various MRS application tools for Alzheimer disease and mild cognitive impairment. American journal of neuroradiology, 2014. 35(6 suppl): p. S4–S11. https://doi.org/10.3174/ajnr.A3944 PMID: 24742809

41. Achtnichts L., et al., Global N-acetylaspartate concentration in benign and non-benign multiple sclerosis patients of long disease duration. Eur J Radiol, 2013. 82(12): p. e848–52. https://doi.org/10.1016/j.ejrad.2013.08.037 PMID: 24041438

42. Brighina E., et al., Human fetal brain chemistry as detected by proton magnetic resonance spectroscopy. Pediatric neurology, 2009. 40(5): p. 327–342. https://doi.org/10.1016/j.pediatrneurol.2008.11.001 PMID: 19380068

43. Horska A., et al., In vivo quantitative proton MRSI study of brain development from childhood to adolescence. J Magn Reson Imaging, 2002. 15(2): p. 137–43. https://doi.org/10.1002/jmri.10057 PMID: 11836768

44. Erecinska M. and Silver I.A., Metabolism and role of glutamate in mammalian brain. Prog Neurobiol, 1990. 35(4): p. 245–96. https://doi.org/10.1016/0301-0082(90)90013-7 PMID: 1980745

45. Danbolt N.C., Glutamate uptake. Prog Neurobiol, 2001. 65(1): p. 1–105. https://doi.org/10.1016/s0301-0082(00)00067-8 PMID: 11369436

46. Sanacora G., et al., Targeting the glutamatergic system to develop novel, improved therapeutics for mood disorders. Nat Rev Drug Discov, 2008. 7(5): p. 426–37. https://doi.org/10.1038/nrd2462 PMID: 18425072

47. Hellem T., et al., The Utility of Magnetic Resonance Spectroscopy for Understanding Substance Use Disorders: A Systematic Review of the Literature. J Am Psychiatr Nurses Assoc, 2015. 21(4): p. 244–75. https://doi.org/10.1177/1078390315598606 PMID: 26282670

48. Xue B., et al., Perinatal Opioid Exposure Results in Persistent Hypoconnectivity of Excitatory Circuits and Reduced Activity Correlations in Mouse Primary Auditory Cortex. J Neurosci, 2022. 42(17): p. 3676–3687. https://doi.org/10.1523/JNEUROSCI.2542-21.2022 PMID: 35332087

49. Zahr N.M., et al., In vivo glutamate measured with magnetic resonance spectroscopy: behavioral correlates in aging. Neurobiol Aging, 2013. 34(4): p. 1265–76.

50. Mersman B., et al., Taurine promotes neurite outgrowth and synapse development of both vertebrate and invertebrate central neurons. Frontiers in Synaptic Neuroscience, 2020. 12: p. 29. https://doi.org/10.3389/fnsyn.2020.00029 PMID: 32792935

51. Cooper A.J. and Kristal B.S., Multiple roles of glutathione in the central nervous system. Biol Chem, 1997. 378(8): p. 793–802. PMID: 9377474

52. Emir U.E., et al., Noninvasive quantification of ascorbate and glutathione concentration in the elderly human brain. NMR Biomed, 2011. 24(7): p. 888–94. https://doi.org/10.1002/nbm.1646 PMID: 21834011

53. Salarian A., et al., Opioid Use Disorder Induces Oxidative Stress and Inflammation: The Attenuating Effect of Methadone Maintenance Treatment. Iran J Psychiatry, 2018. 13(1): p. 46–54. PMID: 29892317

54. Pan J., et al., Oxidative stress in heroin administered mice and natural antioxidants protection. Life Sci, 2005. 77(2): p. 183–93. https://doi.org/10.1016/j.lfs.2004.12.025 PMID: 15862603

55. De Graaf R.A., In vivo NMR spectroscopy: principles and techniques. 2019: John Wiley & Sons.

56. Sung Y.-H., et al., Decreased frontal N-acetylaspartate levels in adolescents concurrently using both methamphetamine and marijuana. Behavioural brain research, 2013. 246: p. 154–161. https://doi.org/10.1016/j.bbr.2013.02.028 PMID: 23466689

57. Iosifescu D.V., et al., Brain bioenergetics and response to triiodothyronine augmentation in major depressive disorder. Biol Psychiatry, 2008. 63(12): p. 1127–34. https://doi.org/10.1016/j.biopsych.2007.11.020 PMID: 18206856

58. Hone-Blanchet A., et al., CO-registration of proton magnetic resonance spectroscopy (1H-MRS) and diffusion imaging (DMRI) in healthy aging: A prospective study of cerebral neurochemistry and microstructure: Neuroimaging/Normal brain aging. Alzheimer's & Dementia, 2020. 16: p. e043251.

59. Grossman E.J., et al., N-acetyl-aspartate levels correlate with intra-axonal compartment parameters from diffusion MRI. Neuroimage, 2015. 118: p. 334–43. https://doi.org/10.1016/j.neuroimage.2015.05.061 PMID: 26037050